Supporting Information

Inhibition of *E. coli* AcrB multidrug efflux pump by MBX2139: molecular mechanism and comparison with other inhibitors.

Attilio V. Vargiu[1], Paolo Ruggerone[1], Timothy J. Opperman[2], Son T. Nguyen[2], and Hiroshi Nikaido[3]

[1]Department of Physics, University of Cagliari, S.P. Monserrato-Sestu Km 0.700, I-09042 Monserrato (CA), Italy

[2]Microbiotix, Inc., Worcester, MA, USA

[3]Department of Molecular and Cell Biology, University of California, Berkeley, CA 94720, USA

Materials and Methods

Simulation Systems.

Compounds. The most likely protonation states of MBX2319 and D13-9001 at pH 7.0 were calculated with the Marvin package (1) following Ref. (2). The force field parameters of these compounds were taken from the GAFF force field (3), and the missing ones were generated using the modules of the AMBER12 package (4). Atomic restrained electrostatic potential (RESP) charges were derived using the antechamber tool of AMBER, after a structural optimization performed with Gaussian09 (5) in the presence of implicit solvent (PCM). The parameters of the other compounds (MIN, PAβN and NMP) were taken from Ref. (2).The parameters of the compounds investigated here are available upon request to the authors.

Docking. The structure of the binary complex AcrB-MBX2319 was generated by docking the ligand into the Binding or B protomer, using the AUTODOCK VINA package (6) and the high-resolution structure of AcrB 2J8S as target (7). A grid of 30 x 30 x 30 Å centered in the middle of the DP was used.

MD simulations. Five simulations (one for each complex) each of more than 300 ns in length were performed using the program NAMD 2.9 (8). A time step of 1.5 fs was used. Periodic boundary conditions were employed, and electrostatic interactions were treated using the particle-mesh-Ewald (PME) method, with a real-space cutoff of 12 Å and a grid spacing of 1 Å per grid point in each dimension. The van der Waals interactions were modeled with a Lennard-Jones potential, using a smooth cutoff (switching radius 10 Å, cutoff radius 12 Å). The simulations were performed in the NPT ensemble and the temperature was kept at 310 K by applying the Langevin thermostat to all heavy atoms with the Langevin damping constant set to

5 ps^{-1}. The pressure was kept at 1.013 bar using the Nosé-Hoover Langevin piston pressure control.

In order to guarantee a slow equilibration phase while keeping the asymmetric structure of the protein in accordance to X-ray data (7, 9, 10) the equilibration and the production runs were performed according to the protocol below (2):

- In order to rearrange the position of waters and ions, relaxation was performed in the presence of soft restraints (1 $kcal \cdot mol^{-1} \cdot Å^{-2}$) on all the non-hydrogenous atoms of the protein and the ligand. In the second and third steps, the restraints were kept only on backbone and Cα atoms, respectively, and on the non-hydrogenous atoms of ligand. Finally, restraints were removed from the ligand and from a selection of residues having at least one atom within 8 Å from the ligand. In all the steps the structure of the solute from previous step was used as target for restraints, and up to 10,000 optimization steps were performed using the conjugate-gradients algorithm.

- Next, annealing up to 350 K was performed in 2 ns, using the same setup as in the last step of the relaxation described at the previous point, and constant volume and temperature conditions (NVT ensemble). This was followed by quenching to 310K in 3 ns, and then a 1 ns long equilibration with same setup as above, but in the NTP ensemble.

- Finally, two productive runs were performed: a) 'partially restrained MD' runs of 15 ns, using the same setup as above, and the last conformation from previous dynamics as target for structural restraints; b) unrestrained MD simulations of ~300 ns, in order to assess further the stability of the ligands within the binding pocket in the absence of any bias. The trajectories were saved every 30 ps, resulting in ~10000 conformations for each trajectory.

Structural relaxation of the trimolecular complexes

The trimolecular adducts MIN-inhibitor-AcrB were generated by docking MIN on the representative average structure of the AcrB-inhibitor complexes extracted from the corresponding MD trajectory. Then, four rounds of partially restrained structural optimization were performed in the presence of soft restraints (1 kcal·mol^{-1}·Å^{-2}). In a first step, the restraints were applied on all the non-hydrogenous atoms of the protein and the ligand. In the second and third steps, the restraints were kept only on backbone and Cα atoms, respectively, and on the non-hydrogenous atoms of ligand. Finally, restraints were removed from the ligand and from a selection of residues having at least one atom within 8 Å from the ligand. In all the steps the structure of the solute from previous step was used as target for restraints, and up to 10,000 optimization steps were performed using the conjugate-gradients algorithm.

Post-processing analyses - free energy evaluation and decomposition into per-residue contributions. The free energy of binding of the inhibitor to AcrB was evaluated by means of the Molecular Mechanics – Generalized Born Surface Area (MM-GBSA) post-processing method (11, 12) using the MMPBSA.py tool of the AmberTools package (13).

According to the MM-GBSA theory, the free energy of binding ΔG_{bind} is evaluated through the following formula:

$$\Delta G_{bind} = G_{com} - \left(G_{rec} + G_{lig}\right).$$

G_{com}, G_{rec}, and G_{lig} are the absolute free energies of complex, receptor, and ligand, respectively, averaged over the equilibrium trajectory of the complex (single trajectory approach). According to these schemes, the free energy difference can be decomposed as:

$$\Delta G_{bind} = \Delta E_{MM} + \Delta G_{solv} - T\Delta S_{conf}$$

where ΔE_{MM} is the difference in the molecular mechanics energy, ΔG_{solv} is the solvation free energy, and $T\Delta S_{conf}$ is the solute conformational entropy. The first two terms were calculated with the following equations:

$$\Delta E_{MM} = \Delta E_{bond} + \Delta E_{angle} + \Delta E_{torsion} + \Delta E_{vdw} + \Delta E_{elec}$$

$$\Delta G_{solv} = \Delta G_{solv,p} + \Delta G_{solv,np}$$

E_{MM} includes the molecular mechanics energy contributed by the bonded (E_{bond}, E_{angle}, and $E_{torsion}$) and non-bonded (E_{vdw} and E_{ele}, calculated with no cutoff) terms of the force field. ΔG_{solv} is the solvation free energy, which can be modeled as the sum of an electrostatic contribution ($\Delta G_{solv,p}$, evaluated using the MM-GBSA approach) and a non-polar one ($\Delta G_{solv,np} = \gamma \Delta_{SA} + b$, proportional to the difference in solvent-exposed surface area, Δ_{SA}).

In the MM-GBSA approach, the electrostatic solvation free energy was calculated using the implicit solvent model in Ref. (14) (igb = 8 option in AMBER12) in combination with mbondi3 (15, 16) (for H, C, N, O, S elements) and intrinsic (17) radii. Partial charges were taken from the AMBER/GAFF force fields, and relative dielectric constants of 1 for solute and 78.4 for the solvent (0.1 M KCl water solution) were used. The non-polar contribution is approximated by the LCPO (18) method implemented within the *sander* module of AMBER. In addition to being faster, the MM-GBSA approach furnishes an intrinsically easy way of decomposing the free energy of binding into contributions from single atoms and residues (19), which is alternative to the “alanine scanning” approach.

Solvation free energies were calculated on ~1000 frames for the unbiased MD simulations. The solute conformational entropy contribution ($T\Delta S_{conf}$) is composed by a rototranslational term,

calculated through classical statistical mechanics formulas, and by a vibrational term, which has been estimated here through normal-mode analysis using the *nmode* module of AMBER. To reduce the errors in the evaluation of the entropic term and to speed up the calculation of the vibrational contribution to ΔS, we followed a recently developed approach (20) also used in previous works by some of us (2, 21, 22). In this method, normal modes calculations are performed on a subset of atoms of the system (namely those belonging to residues within 8 Å of the ligand), but in the presence of a buffer region containing protein residues between 8 and 12 Å from the inhibitor and water molecules within 12 Å of the ligand. This avoids large distortions of the structure with respect to the conformation extracted from the dynamics, and the questionable use of a distance-dependent dielectric constant. The cutoff on the convergence on the forces was set to 10^{-5} kcal/(mol·Å). Solute entropies were calculated, for each system, on ~300 snapshots taken every t_{eq}/300 ps from the part of the unbiased trajectories of length t_{eq} selected for all the analyses reported here (see Fig. S1).

Post-processing analyses - surface matching within the AcrB pockets. The software PLATINUM (23) was used to get an estimate of the binding affinity of various compounds to the distal and proximal pocket. The method is based on the concept of empirical molecular hydrophobicity potential (MHP (24)), which is used to calculate molecular hydrophobic/hydrophilic properties. Namely, the MHP at any point *j*, due to N atoms, is defined as (25, 26):

$$MHP_j = \sum_{i=1}^{N} f_i \cdot d(r_{ij})$$

where i and f_i are the atom number and the corresponding hydrophobicity constant, and $d(r_{ij})$ is the distance function between atom i and point j. In our calculations we selected the Fermi-like function:

$$d(r_{ij}) = \frac{\left[1 + e^{\alpha r_{ij} - c}\right]^{-1}}{\sum_{k=1}^{N}\left[1 + e^{\alpha r_{ik} - c}\right]^{-1}}$$

where c is a cutoff, usually set to 4 Å, and a = 1 Å^{-1}. The atomic hydrophobicity constants (~120 atom types were available) are derived from octanol-water log P values for various organic compounds (27) and automatically assigned according to the molecular topology. Positive and negative MHP values correspond respectively to hydrophobic and hydrophilic surface regions. Comparison of molecular MHPs on the interfacial surface gives an understanding of the complementarity of the ligand to the receptor's binding site in terms of hydrophobic and hydrophilic matching (23, 25, 26). Specifically, the complementarity between AcrB and the ligand is estimated by the matching of hydrophobic and hydrophilic areas, projected for both partners onto the Connolly surface of the ligand, and calculated as:

$$M_L = \frac{2S_{LL}}{2S_{LL} + S_{HL} + S_{LH} + S_{LW}}$$

The lipophilic matching M_L is particularly significant in the case of AcrB, since all of its substrates share a certain degree of lipophilicity (28, 29). This is confirmed by the analysis of hydrophobic vs hydrophilic surfaces of the compounds investigated here (Table 1). Furthermore, it has already been reported (and rationalized through MHP calculations) that a variety of hydrophobic interactions (which are not as directional as salt bridges or H-bonds) plus some weak polar groups are characteristics of binding pockets able to interact with structurally diverse substrates (30).

The analyses as well as the atomic-level figures, were performed using *tcl* scripts within VMD (31) or utilities of the AMBER package.

SUPPLEMENTARY TABLES

Compound	Biased MD (ns)	Unbiased MD (ns)
MBX2319	17	300
NMP	17	300
PAβN	22	300
D13-9001	17	300
MIN	17	300

Table S1. Length of MD simulations performed in this work.

Compound	Mol. Weight	Net Charge[b]	# HB acceptors	# HB donors	Hydrophobic surface (%)[c]	LogP[d]
MIN	457.5	0	9	5	58	0.90
MBX2319	409.5	0	5	0	95	3.76
D13-9001	694.8	-1	12	2	68	1.94
PAβN	448.6	+2	4	6	49	1.98
NMP	227.3	+1	1	1	66	2.44
DOX	543.2	0	11	6	67	1.27

[a] Inhibitors of the pump are italicized.
[b] The most likely protonation state at pH=7.0 has been calculated for each compound using the Marvin(1) package
[c] Calculated with the program PLATINUM (23)
[d] Calculated with XLogP3 (32)

Table S2. Physico-chemical properties of the inhibitor subject of the present study, compared to those of selected compounds from Ref. (2). The names of inhibitors are italicized.

Residue	***MBX2319***	***D13-9001***	***NMP***	***PAβN***	***DOX$_{F610A}$***	**MIN**
T44	-	-	-	-0.6 (0.5)	-	-
S46	-	-	-	-	-0.7 (1.1)	-
S48	-	-	-	-	-	-1.2 (0.9)
Q89	-	-	-	-1.3 (1.0)	-0.6 (1.1)	-
S128	-	-1.4 (1.5)	-	-	-	-
E130	-	-	-	-0.7 (1.9)	-	-
F136	-2.1 (0.5)	-1.0 (0.4)	-1.7 (0.6)	-1.7 (0.5)	-2.8 (0.6)	-
V139	-1.1 (0.4)	-1.6 (0.3)	-	-	-1.0 (0.2)	-
Q151	-	-1.3 (0.5)	-	-	-	-0.8 (0.5)
S155	-	-3.4 (0.9)	-	-	-	-
Q176	-	-	-1.1 (0.6)	-2.5 (0.6)	-1.7 (0.6)	-
L177	-	-0.7 (0.6)	-	-	-1.3 (0.8)	-
F178	-0.7 (0.6)	-5.7 (0.8)	-0.7 (0.6)	-1.0 (0.5)	-3.1 (0.8)	-2.5 (0.5)
G179	-	-2.3 (0.7)	-	-	-	-1.0 (0.4)
S180	-	-0.8 (1.2)	-	-	-	-0.8 (0.4)
N274	-	-	-	-	-	-1.4 (1.1)
I277	-	-2.3 (0.5)	-	-0.9 (0.5)	-0.7 (0.4)	-3.3 (0.6)
I278	-	-	-	-	-	-0.6 (0.2)
A279	-	-1.0 (0.4)	-	-	-	-
S287	-	-0.6 (0.4)	-	-	-	-
G288	-	-4.3 (0.9)	-	-	-	-
P326	-	-0.8 (0.3)	-	-	-	-
Y327	-2.3 (0.6)	-1.5 (0.4)	-	-	-0.8 (0.4)	-
V571	-1.2 (0.4)	-0.6 (0.2)	-	-	-	-
M573	-0.7 (0.5)	-0.6 (0.2)	-	-	-	-
F/A610	-1.3 (0.7)	-2.7 (0.5)	-	-	-	-
V612	-	-1.5 (0.3)	-	-	-	-1.0 (0.3)
F615	-	-1.9 (0.4)	-1.5 (0.5)	-3.3 (0.5)	-1.6 (0.4)	-1.0 (0.3)
F617	-	-	-	-	-0.7 (0.8)	-
A618	-	-	-0.9 (0.5)	-0.7 (0.5)	-	-
R620	-	-	-	-	-0.9 (0.3)	-0.7 (1.3)
I626	-	-	-1.0 (0.6)	-0.6 (0.5)	-	-
F628	-3.8 (0.6)	-3.7 (0.5)	-1.1 (0.6)	-0.8 (0.4)	-0.6 (0.4)	-
L668	-1.7 (0.5)	-	-	-	-	-
V672	-0.7 (0.3)	-	-	-	-	-
E673	-	-	-	-0.9 (0.8)	-	-

Table S3. Relevant per-residue contributions to ΔG_b for the inhibitor MBX2319, compared with results for inhibitors NMP, PAβN(2) and D13-9001 (33), with the substrate MIN and with the substrate DOX in the F610A variant of AcrB. Only residues contributing more than kT at room temperature (0.593 kcal/mol) are reported. Residues contributing to binding of two or more inhibitors are bolded, and those contributing to binding of all inhibitors are also italicized.

Residues belonging to the “hydrophobic trap” defined in Ref. (33) are underlined and the corresponding row shared gray in the Table.

SUPPLEMENTARY FIGURES

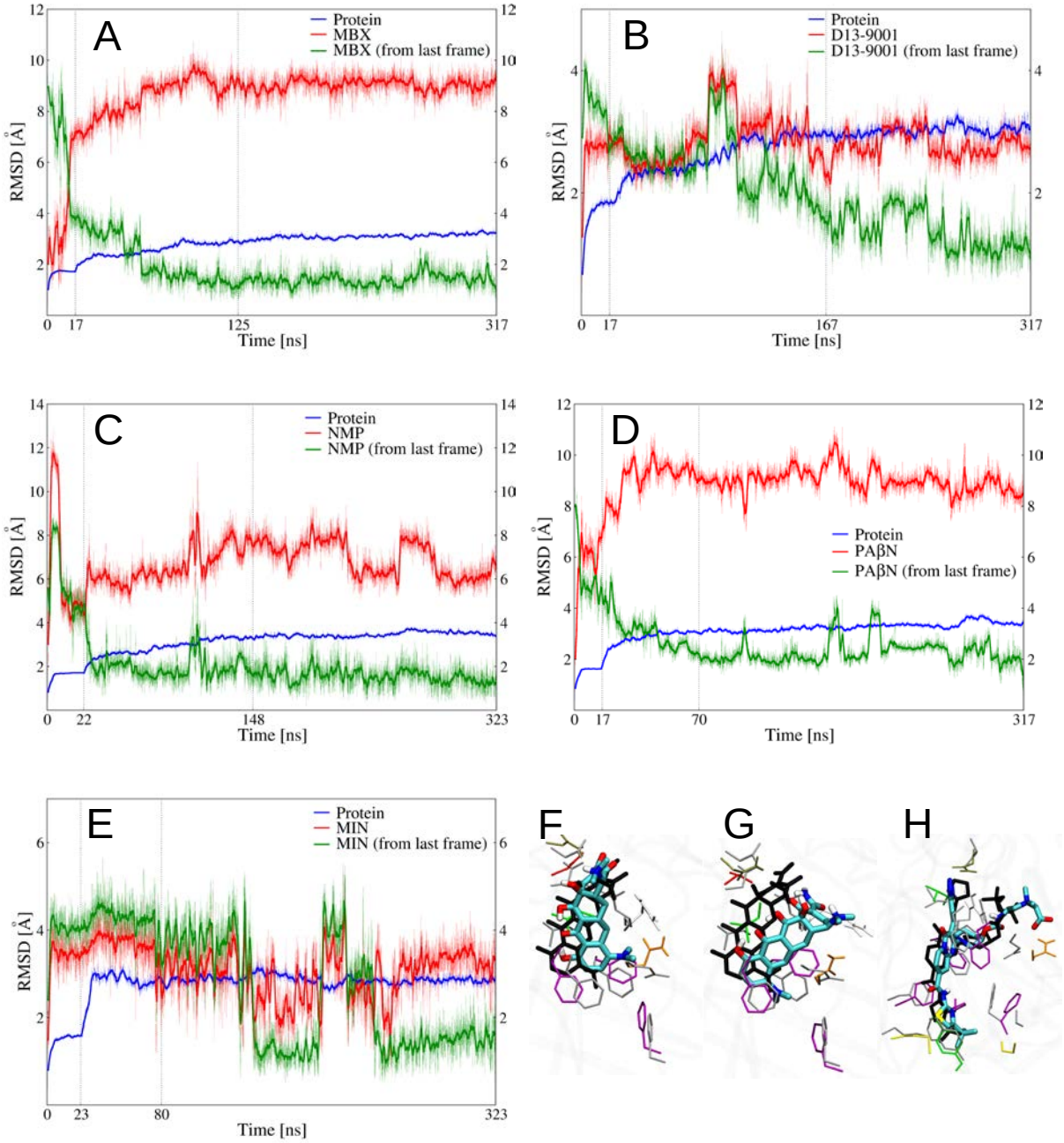

Figure S1. A-E) RMSD profiles along the trajectory of each system simulated in this work. The profiles of the protein and of the ligands with respect to the docking structure are shown by blue and red curves respectively, while the RMSD of the ligands with respect to the last snapshot of the trajectory is shown with a green curve. The solid lines represent running averages over 50 points of the dotted lines; F-G) Comparison between two representative conformations extracted

from the MD trajectory of AcrB-MIN (the drug is shown in thick sticks colored according to the atom type, and residues within 3.5 Å are represented by thin sticks colored according to the residue type) and the X-ray structure in Ref. (34) (PDB code 4DX5); H) Comparison between a representative conformation extracted from the MD trajectory of AcrB-D13-9001 and the X-ray structure in Ref. (33) (PDB code 3W9H).

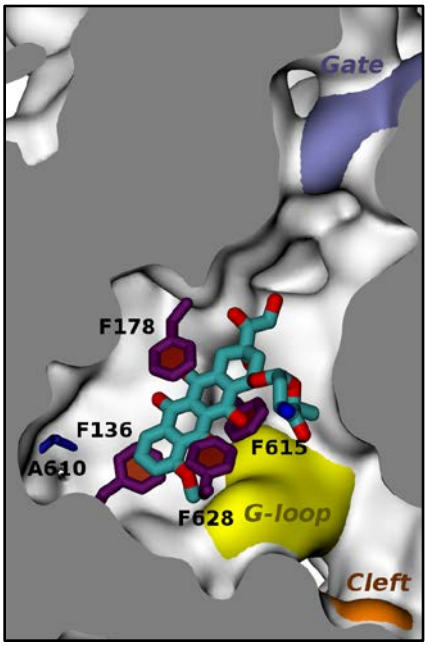

Figure S2. Position of DOX with respect to the hydrophobic trap in monomer B of the F610A variant of AcrB. The ligand is shown in tick sticks colored according to the atom type, and the side chains of residues constituting the hydrophobic trap are shown with sticks (thick if the residue is within 3.5 Å of the ligand, thinner otherwise). The rest of the protein is shown with molecular surface, colored in orange, yellow and iceblue at the PC1/PC2 Cleft, the G-loop tip and the exit Gate respectively, and white elsewhere. No channels leading from the Cleft to the Gate through the AP and/or DP were found in this complex.

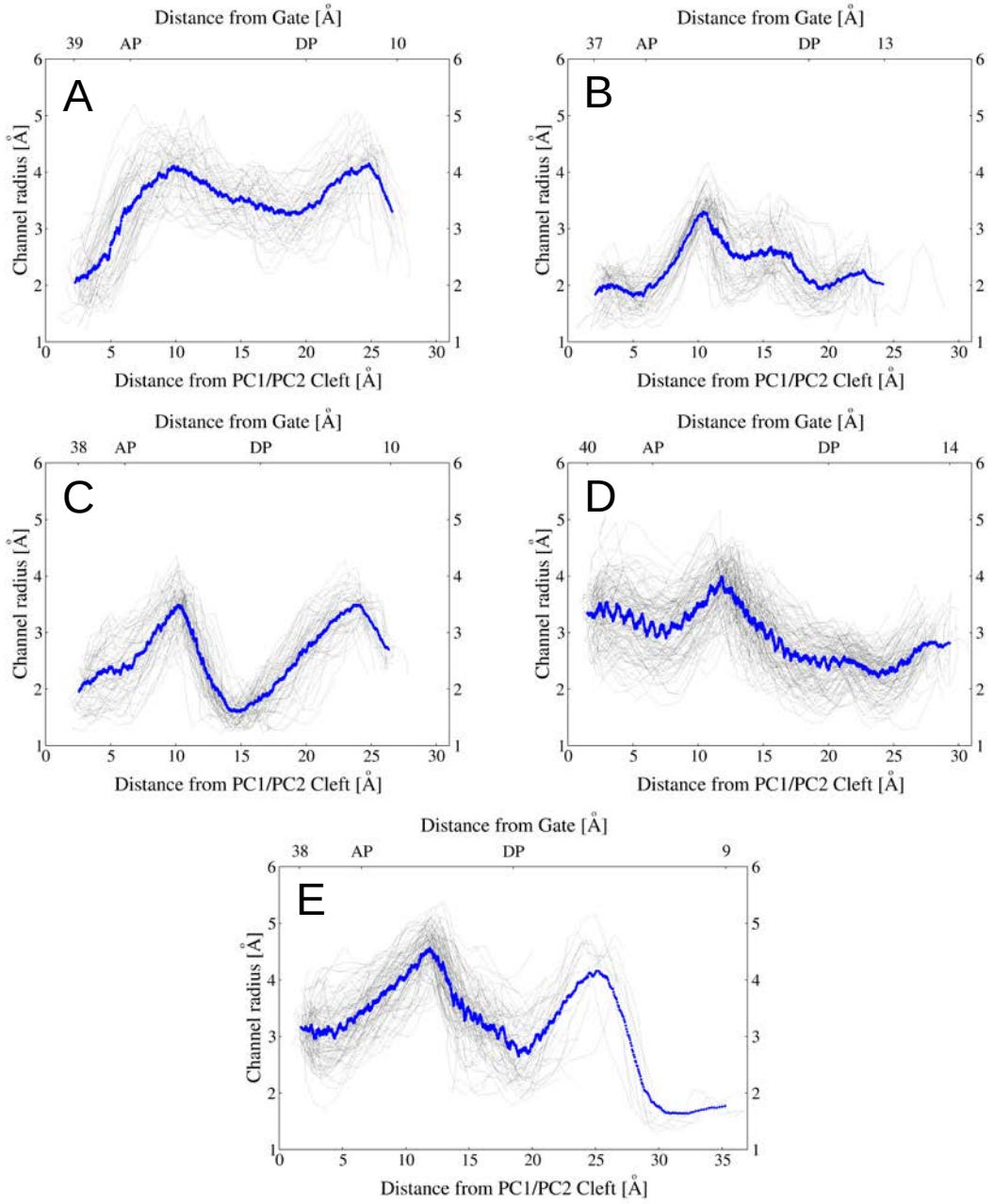

Figure S3. Radii of the channels leading from the PC1/PC2 Cleft to the exit Gate as found in the adducts between AcrB and MBX2319 (A), D13-9001 (B), NMP (C), MIN (D), and in the transporter free of ligands (E). As reported in the main text, no channel was found in the AcrB-PAβN complex. The tiny black lines in each graph represent the profiles of the radii as extracted from ~120 snapshots of MD trajectory with the program CAVER (35), while the running average over 50 steps of the whole set of data is represented by blue solid circles.

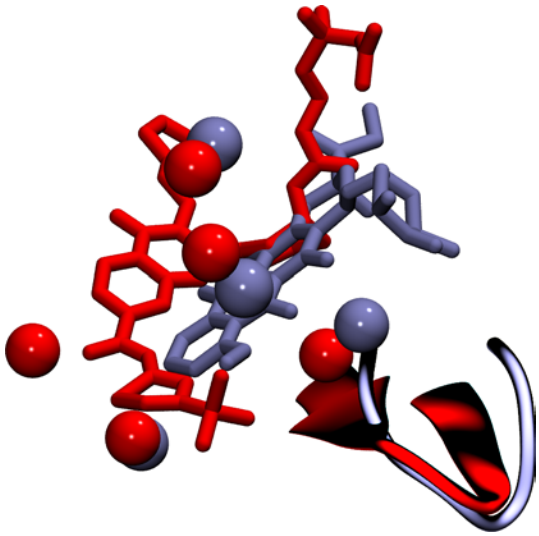

Figure S4. Superimposition between representative structures of D13-9001 (red sticks) and DOX (iceblue) within the hydrophobic trap of AcrB and $AcrB_{F610A}$ respectively. The residues of the trap within 3.5 Å of the ligands are shown by solid spheres, while the tips of the G-loop are shown in cartoons.

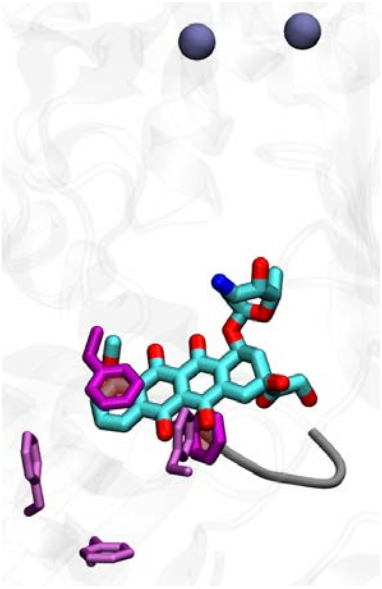

Figure S5. Position of DOX relative to the hydrophobic trap in the highest resolution structure available to date of the ligand in complex with AcrB (34). The drug is shown in thick sticks colored according to the atom type, with the sidechains of residues lining the trap and within 3.5 Å of DOX represented by thick magenta sticks, while the other residues of the trap are shown thinner. The protein is shown in transparent cartoon representation, except for the tip of the G-loop shown in solid gray. The residues Q124 and Y758 lining the exit Gate are shown by iceblue solid spheres.

References

1. 2012. Marvin, 2.5.9 ed. ChemAxon.
2. **Vargiu AV, Nikaido H.** 2012. Multidrug binding properties of the AcrB efflux pump characterized by molecular dynamics simulations. Proc. Natl. Acad. Sci. U.S.A. **109:**20637-20642.
3. **Wang J, Wolf RM, Caldwell JW, Kollman PA, Case DA.** 2004. Development and testing of a general amber force field. J. Comput. Chem. **25:**1157-1174.
4. **Case DA, Darden TA, Cheatham III TE, Simmerling CL, Wang J, Duke RE, Luo R, Walker RC, Zhang W, Merz KM, Roberts B, Hayik S, Roitberg A, Seabra G, Swails J, Goetz AW, Kolossvai I, Wong KF, Paesani F, Vanicek J, Wolf RM, Liu J, Wu X, Brozell SR, Steinbrecher T, Gohlke H, Cai Q, Ye X, Wang J, Hsieh M-J, Cui G, Roe DR, Mathews DH, Seetin MG, Salomon-Ferrer R, Sagui C, Babin V, Luchko T, Gusarov S, Kovalenko A, Kollman PA.** 2012. AMBER12. University of California, San Francisco.
5. **Frisch MJ, Trucks GW, Schlegel HB, Scuseria GE, Robb MA, Cheeseman JR, Scalmani G, Barone V, Mennucci B, Petersson GA, Nakatsuji H, Caricato M, Li X, Hratchian HP, Izmaylov AF, Bloino J, Zheng G, Sonnenberg JL, Hada M, Ehara M, Toyota K, Fukuda R, Hasegawa J, Ishida M, Nakajima T, Honda Y, Kitao O, Nakai H, Vreven T, Jr. JAM, Peralta JE, Ogliaro F, Bearpark M, Heyd JJ, Brothers E, Kudin KN, Staroverov VN, Kobayashi R, Normand J, Raghavachari K, Rendell A, Burant JC, Iyengar SS, Tomasi J, Cossi M, Rega N, Millam JM, Klene M, Knox JE, Cross JB, Bakken V, Adamo C, Jaramillo J, Gomperts R, Stratmann RE, Yazyev O, Austin AJ, Cammi R, Pomelli C, Ochterski JW, Martin RL, Morokuma K, Zakrzewski VG, Voth GA, Salvador P, Dannenberg JJ, Dapprich S, Daniels AD, Farkas Ö, Foresman JB, Ortiz JV, Cioslowski J, Fox DJ.** 2009. Gaussian 09, Revision A.1, Revision A.1 ed. Gaussian, Inc., Wallingford CT.
6. **Trott O, Olson AJ.** 2010. Autodock Vina: Improving the Speed and Accuracy of Docking with a New Scoring Function, Efficient Optimization, and Multithreading. J. Comput. Chem. **31:**455-461.
7. **Sennhauser G, Amstutz P, Briand C, Storchenegger O, Grutter MG.** 2007. Drug export pathway of multidrug exporter AcrB revealed by DARPin inhibitors. PLoS Biology **5:**106-113.
8. **Phillips JC, Braun R, Wang W, Gumbart J, Tajkhorshid E, Villa E, Chipot C, Skeel RD, Kale L, Schulten K.** 2005. Scalable molecular dynamics with NAMD. J. Comput. Chem. **26:**1781-1802.
9. **Seeger MA, Schiefner A, Eicher T, Verrey F, Diederichs K, Pos KM.** 2006. Structural Asymmetry of AcrB Trimer Suggests a Peristaltic Pump Mechanism. Science **313:**1295-1298.
10. **Murakami S, Nakashima R, Yamashita E, Matsumoto T, Yamaguchi A.** 2006. Crystal structures of a multidrug transporter reveal a functionally rotating mechanism. Nature **443:**173-179.
11. **Kollman Pa, Massova I, Reyes C, Kuhn B, Huo S, Chong L, Lee M, Lee T, Duan Y, Wang W, Donini O, Cieplak P, Srinivasan J, Case Da, Cheatham TE.** 2000. Calculating structures and free energies of complex molecules: combining molecular mechanics and continuum models. Acc. Chem. Res. **33:**889-897.

12. **Srinivasan J, Cheatham III TE, Cieplak P, Kollman PA, Case DA.** 1998. Continuum Solvent Studies of the Stability of DNA, RNA, and Phosphoramidate-DNA Helices. J. Am. Chem. Soc. **120:**9401-9409.
13. **Miller BR, McGee TD, Swails JM, Homeyer N, Gohlke H, Roitberg AE.** 2012. MMPBSA.py: An Efficient Program for End-State Free Energy Calculations. J. Chem. Theory Comp. **8:**3314-3321.
14. **Shang Y, Nguyen H, Wickstrom L, Okur A, Simmerling C.** 2011. Improving the description of salt bridge strength and geometry in a Generalized Born model. J. Mol. Graph. **29:**676-684.
15. **Onufriev A, Bashford D, Case DA.** 2004. Exploring protein native states and large-scale conformational changes with a modified generalized born model. Proteins **55:**383-394.
16. **Bondi A.** 1964. van der Waals Volumes and Radii. J. Phys. Chem. **68:**441-451.
17. **Tsui V, Case DA.** 2000. Molecular dynamics simulations of nucleic acids with a generalized born solvation model. J. Am. Chem. Soc. **122:**2489-2498.
18. **Weiser J, Shenkin PS, Still WC.** 1999. Approximate atomic surfaces from linear combinations of pairwise overlaps (LCPO). J. Comput. Chem. **20:**217-230.
19. **Gohlke H, Kiel C, Case DA.** 2003. Insights into Protein–Protein Binding by Binding Free Energy Calculation and Free Energy Decomposition for the Ras–Raf and Ras–RalGDS Complexes. J. Mol. Biol. **330:**891-913.
20. **Kongsted J, Ryde U.** 2009. An improved method to predict the entropy term with the MM/PBSA approach. J. Comput.-Aided Mol. Des. **23:**63-71.
21. **Asthana S, Shukla S, Vargiu AV, Ceccarelli M, Ruggerone P, Paglietti G, Marongiu ME, Blois S, Giliberti G, La Colla P.** 2013. Different Molecular Mechanisms of Inhibition of Bovine Viral Diarrhea Virus and Hepatitis C Virus RNA-Dependent RNA Polymerases by a Novel Benzimidazole. Biochemistry **52:**3752-3764.
22. **Kinana AD, Vargiu AV, Nikaido H.** 2013. Some Ligands Enhance the Efflux of Other Ligands by the Escherichia coli Multidrug Pump AcrB. Biochemistry **52:**8342-8351.
23. **Pyrkov TV, Chugunov AO, Krylov NA, Nolde DE, Efremov RG.** 2009. PLATINUM: a web tool for analysis of hydrophobic/hydrophilic organization of biomolecular complexes. Bioinformatics **25:**1201-1202.
24. **Audry E, Dubost JP, Colleter JC, Dallet P.** 1986. A new approach of structure activity relationships: The 'potential of molecular lipophilicity'. Eur. J. Med. Chem. **21:**71-72.
25. **Pyrkov TV, Kosinsky YA, Arseniev AS, Priestle JP, Jacoby E, Efremov RG.** 2007. Complementarity of hydrophobic properties in ATP-protein binding: A new criterion to rank docking solutions. Proteins **66:**388-398.
26. **Efremov RG, Chugunov AO, Pyrkov TV, Priestle JP, Arseniev AS, Jacoby E.** 2007. Molecular lipophilicity in protein modeling and drug design. Curr. Med. Chem. **14:**393-415.
27. **Ghose AK, Viswanadhan VN, Wendoloski JJ.** 1998. Prediction of hydrophobic (lipophilic) properties of small organic molecules using fragmental methods: An analysis of ALOGP and CLOGP methods. J. Phys. Chem. A **102:**3762-3772.
28. **Nikaido H.** 2011. Structure and Mechanism of RND-Type Multidrug Efflux Pumps, p. 1-60, Adv. Enzymol. Relat. Areas Mol. Biol., vol. 77. John Wiley & Sons, Inc.

29. **Ruggerone P, Murakami S, Pos KM, Vargiu AV.** 2013. RND Efflux Pumps: Structural Information Translated into Function and Inhibition Mechanisms. Curr. Top. Med. Chem. **13:**3079-3100.
30. **Vistoli G, Pedretti A, Mazzolari A, Testa B.** 2010. In silico prediction of human carboxylesterase-1 (hCES1) metabolism combining docking analyses and MD simulations. Bioorg. Med. Chem. **18:**320-329.
31. **Humphrey W, Dalke A, Schulten K.** 1996. VMD: visual molecular dynamics. J. Mol. Graph. **14:**33-38.
32. **Cheng T, Zhao Y, Li X, Lin F, Xu Y, Zhang X, Li Y, Wang R, Lai L.** 2007. Computation of Octanol-Water Partition Coefficients by Guiding an Additive Model with Knowledge. J. Chem. Inf. Model. **47:**2140-2148.
33. **Nakashima R, Sakurai K, Yamasaki S, Hayashi K, Nagata C, Hoshino K, Onodera Y, Nishino K, Yamaguchi A.** 2013. Structural basis for the inhibition of bacterial multidrug exporters. Nature **500:**102-106.
34. **Eicher T, Cha H-j, Seeger MA, Brandstätter L, El-Delik J, Bohnert JA, Kern WV, Verrey F, Grütter MG, Diederichs K, Pos KM.** 2012. Transport of drugs by the multidrug transporter AcrB involves an access and a deep binding pocket that are separated by a switch-loop. Proc. Natl. Acad. Sci. U.S.A.
35. **Chovancova E, Pavelka A, Benes P, Strnad O, Brezovsky J, Kozlikova B, Gora A, Sustr V, Klvana M, Medek P, Biedermannova L, Sochor J, Damborsky J.** 2012. CAVER 3.0: A Tool for the Analysis of Transport Pathways in Dynamic Protein Structures. PLoS Comput. Biol. **8:**e1002708.